easy to assess rate constants for O_2^- reactions with the viologens ($k_{-10} \equiv k_{O_2^-}$). These values (M^{-1} s^{-1}) and those for the ratio log $k_{SO_2^-}/k_{O_2^-}$ for the four viologens are as follows: DQ^{2+} 3.0×10^5, 2.3; MV^{2+} 1.0×10^4, 3.0; PDQ^{2+} 2.4×10^2, 3.1; and BDQ^{2+} 7.7, 3.0. The constant ratio (of approximately 10^3 for rate constants for reaction of SO_2^- and O_2^- with a common oxidant) is striking, and these can be added to a substantial list already compiled.[3]

Acknowledgment. We are grateful to the National Science Foundation for a grant to support this work. We appreciate the considerable assistance of Dr. Stephen J. Atherton in carrying out the pulse radiolysis experiments at the Center for Fast Kinetics Research, The University of Texas, Austin, TX 78712. The Center is supported jointly by the Biotechnology Branch of the Division of Research Resources of NIH (RR 00886) and by the University of Texas at Austin.

Registry No. 1a, 15302-80-4; **1a** (radical cation), 95617-21-3; **1b**, 15302-81-5; **1b** (radical cation), 95617-20-2; **2a**, 2764-72-9; **2a** (radical cation), 63406-50-8; **2b**, 16651-71-1; **2b** (radical cation), 94887-40-8; **2c**, 7325-63-5; **2c** (radical cation), 67509-62-0; **2d**, 16651-68-6; **2d** (radical cation), 67509-63-1; **3a** (radical cation), 25239-55-8; **3b**, 13096-46-3; **3b** (radical cation), 49765-27-7; sulfur dioxide radical anion, 12143-17-8; dithionite, 14844-07-6; sodium dithionite, 7775-14-6; methyl viologen, 1910-42-5.

Supplementary Material Available: Kinetic data for reduction of viologens with dithionite and obseration wavelengths (3 pages). Ordering information is given on any current masthead page.

^{14}N and ^{15}N ENDOR Studies of Intrabridgehead Three-Electron σ-Bonded Radical Cations. Observation of Second-Order Splittings

B. Kirste,[1a] R. W. Alder,[1b] R. B. Sessions,[1b] M. Bock,[1a] H. Kurreck,*[1a] and S. F. Nelsen[1c]

Contribution from the Institut für Organische Chemie, Freie Universität Berlin, 1000 Berlin 33, West Germany, the School of Chemistry, University of Bristol, Bristol BS8 1TS, England, and the Department of Chemistry, University of Wisconsin, Madison, Wisconsin 53706.
Received August 27, 1984

Abstract: EPR, ^1H, ^{14}N, and ^{15}N ENDOR and TRIPLE resonance measurements performed on intrabridgehead three-electron σ-bonded radical cations generated from 1,6-diazabicyclo[4.4.4]tetradecane and the doubly ^{15}N-labeled compound are reported. All evidence obtained supports the view that the N–N bond is truly symmetrical. Pronounced second-order splittings have been observed in the ^{14}N and ^{15}N ENDOR spectra owing to equivalent nuclei with large hyperfine coupling constants. It is shown that the measured second-order effects are in full agreement with theory. Relative signs of the hyperfine couplings have been determined by TRIPLE resonance and by the interpretation of cross-relaxation effects. The influence of the negative sign of the gyromagnetic ratio of the ^{15}N nucleus on the second-order shifts and the cross-relaxation effects is demonstrated.

Bicyclic diamines built from medium-sized rings and containing bridgehead nitrogen atoms show unusual physical and chemical properties due to the enforced interaction of the nitrogen lone pairs imposed by the ring systems.[2-4] In this paper we report on ^1H, ^{14}N, and ^{15}N ENDOR studies of the radical cation of 1,6-diazabicyclo [4.4.4]tetradecane (**1**) and of the doubly ^{15}N labeled species (**2**).

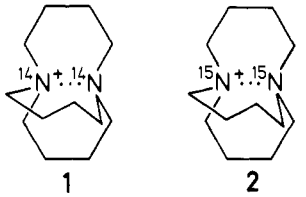

1 **2**

These propellane-type radical cations are interesting for their bonding properties and their structures. The N–N bond in **1** is probably best described as a three-electron σ bond, and the σ^* character of the spin-bearing orbital gives rise to a large ^{14}N hyperfine coupling ($a_{^{14}N}$ = 96.4 MHz).[3] In particular, it is a challenge to find out whether these species are truly symmetrical. The two nitrogen atoms in **1** should be equivalent either if the radical cation has a symmetrical equilibrium structure or if the radical cation is rapidly interconverting between two unsymmetrical structures.

Whereas the EPR spectrum of **1** indicates that the two nitrogen atoms are indeed equivalent,[3] the ENDOR spectrum should provide a much more accurate test of this assumption owing to the higher resolving power of ENDOR spectroscopy. However, in view of the extraordinarily large value of the ^{14}N hyperfine coupling constant, it may be expected that the ENDOR spectrum will be complicated by significant second-order effects. It has long been recognized that ENDOR signals belonging to sets of equivalent nuclei with large coupling constants should exhibit splittings due to second-order effects.[5] Whereas the appearance of second-order frequency *shifts* of ENDOR signals has been observed occasionally,[6] experimental evidence for second-order *splittings* in ENDOR-in-solution spectra was lacking hitherto.[7]

(1) (a) Freie Universität Berlin. (b) University of Bristol. (c) University of Wisconsin.
(2) Alder, R. W.; Goode, N. C.; King, T. J.; Mellor, J. M.; Miller, B. W. *J. Chem. Soc., Chem. Commun.* **1976**, 173. Alder, R. W.; Gill, R.; Goode, N. C. *Ibid.* **1976**, 973. Alder, R. W.; Sessions, R. B.; Mellor, J. M.; Rawlins, M. F. *Ibid.* **1977**, 747.
(3) Alder, R. W.; Sessions, R. B. *J. Am. Chem. Soc.* **1979**, *101*, 3651.
(4) Alder, R. W.; Sessions, R. B.; Bennet, A. J.; Moss, R. E. *J. Chem. Soc., Perkin Trans. 1* **1982**, 603.
(5) Maki, A. H.; Allendoerfer, R. D.; Danner, J. C.; Keys, R. T. *J. Am. Chem. Soc.* **1968**, *90*, 4225.
(6) Leniart, D. S.; Vedrine, J. C.; Hyde, J. S. *Chem. Phys. Lett.* **1970**, *6*, 637.
(7) Very recently, second-order splittings of methylene proton ENDOR signals have been reported. Evans, J. C.; Obaid, A. Y.; Rowlands, C. C., paper presented at the 16th International Conference on ESR of Radicals in Organic and Bio-organic Systems, Oxford, 1984. Evans, J. C.; Obaid, A. Y.; Rowlands, C. C. *Chem. Phys. Lett.* **1984**, *109*, 398.

0002-7863/85/1507-2635$01.50/0

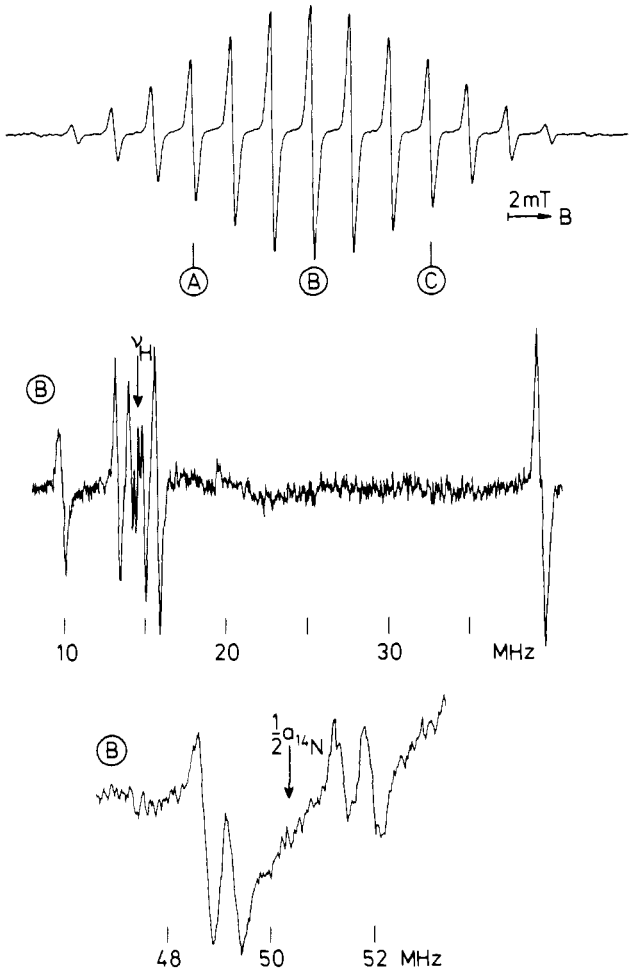

Figure 1. EPR (top), ^1H ENDOR (center), and ^{14}N ENDOR (bottom) spectra of **1** (toluene/CF_3COOH; EPR: 290 K, ENDOR: 230 K).

Table I. Hyperfine Coupling Constants (MHz) of **1** (**2**)

	230 K toluene/CF_3COOH	160 K CH_2Cl_2
^{14}N (2 N)	+100.7	
^{15}N (2 N)	−141.0	
^1H (6 H)	+49.41	+49.36
^1H	+2.40	+2.22
^1H	−0.78	−0.79
^1H	−0.28	−0.29
g	2.00290	

Regarding the radical cation **1**, it should be possible to discriminate between second-order splittings and splittings caused by a perturbation of the symmetry by comparison with the isotopically labeled species **2**.

Results and Discussion

^1H and ^{14}N ENDOR and TRIPLE. Figure 1 shows EPR, ^1H, and ^{14}N ENDOR spectra of **1**.[8] It is noteworthy that one of the proton coupling constants is extraordinarily large. According to the ENDOR resonance condition

$$\nu_{ENDOR} = |\nu_n \pm a/2| \quad (1)$$

the respective ENDOR signals are centered about $|a/2|$, spaced by twice the free proton resonance frequency, $2\nu_H$, because $|a/2| > \nu_H$. Three pairs of ^1H ENDOR lines belonging to smaller couplings appear equally spaced about the free proton frequency (ν_H = 14.66 MHz). Moreover, the ^1H ENDOR signal at the highest frequency exhibits a slight splitting (≈0.19 MHz) which is real in the sense that it is not due to a coherence effect[9] as could be proven by reducing the radio-frequency power level. The separation between the respective low- and high-frequency signals (29.44 MHz) is actually somewhat larger than $2\nu_H$ because of second-order shifts (vide infra). Relative signs of the proton coupling constants have been determined by general TRIPLE resonance experiments,[10] and the data are collected in Table I.

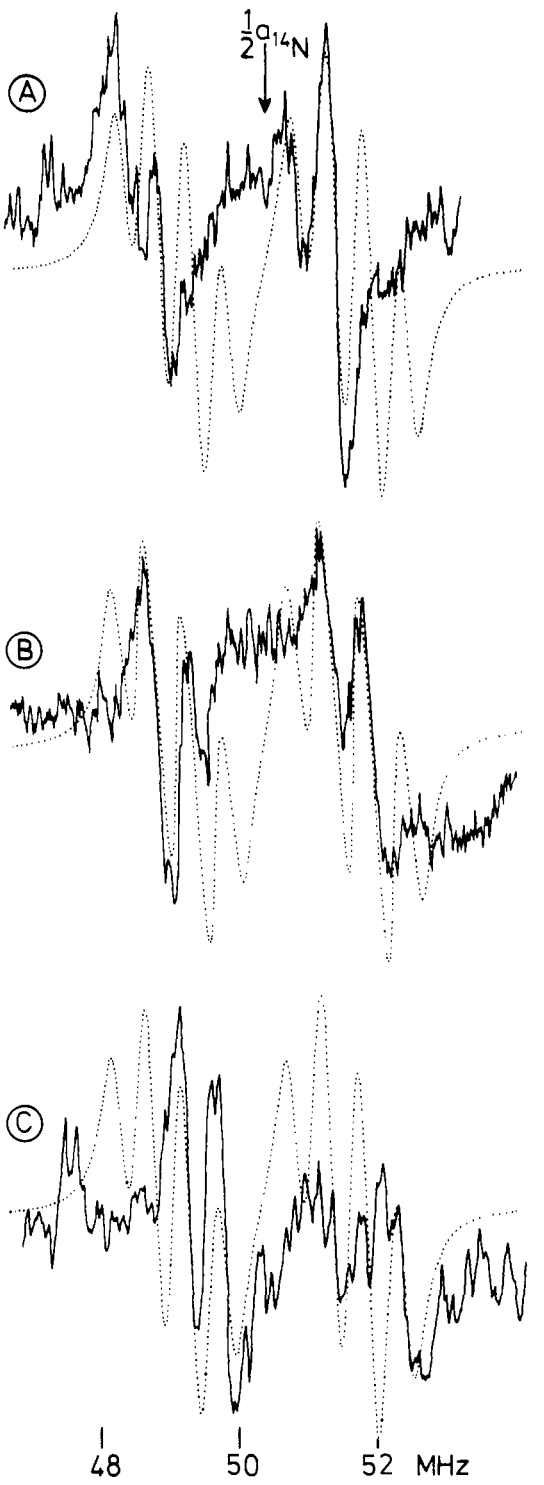

Figure 2. ^{14}N ENDOR spectra of **1** obtained with different field settings, cf. Figure 1 (top): (A) low-, (B) center-, and (C) high-field setting (toluene/CF_3COOH, 230 K). The dotted spectra are computer simulations, see text.

(8) ^1H ENDOR data for **1** have been obtained previously by F. Gerson, Basel. See ref 3.

(9) Freed, J. H.; Leniart, D. S.; Hyde, J. S. *J. Chem. Phys.* **1967**, *47*, 2762. Dinse, K. P.; Möbius, K.; Biehl, R. *Z. Naturforsch. A* **1973**, *A28*, 1069.

(10) Möbius, K.; Biehl, R. In "Multiple Electron Resonance Spectroscopy"; Dorio, M. M.; Freed, J. H., Eds.; Plenum Press: New York, 1979; p 475.

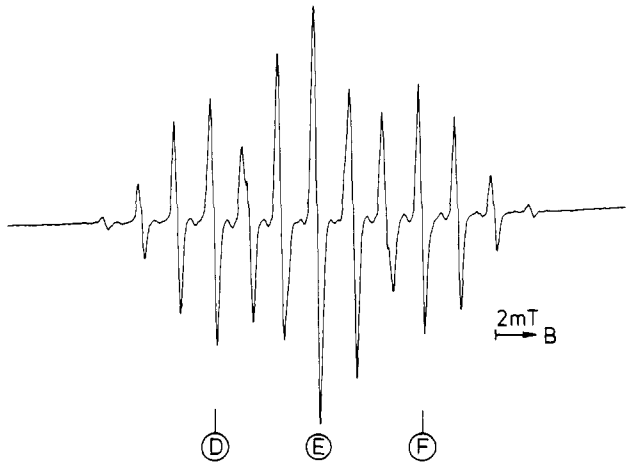

Figure 3. EPR spectrum of **2** (CH_2Cl_2, 230 K).

The ^{14}N ENDOR spectrum of **1** depicted in Figure 1 (bottom), obtained with a field setting on the central peak of the EPR spectrum (B), shows two pairs of signals centered about an "average" $|a_{^{14}N}/2| = 50.36$ MHz. The splitting between the two low- or high-frequency signals amounts to 0.56 MHz. Moreover, pronounced shifts of the ^{14}N ENDOR signal positions are found when the field setting is shifted to a low- (A) or a high-field (C) EPR component (see Figure 2). Also the relative signal intensities depend on the field setting, i.e., the high-frequency ENDOR lines are more intense with the low-field setting (A), whereas the low-frequency lines are more intense with the high-field setting (C). A discussion of these phenomena will be given below.

^{15}N ENDOR. The EPR spectrum of the ^{15}N-labeled species **2** (Figure 3) exhibits a hyperfine pattern consisting of a triplet of overlapping septets. The large triplet splitting (5.03 mT) is due to hyperfine interaction with two ^{15}N nuclei. Since the sample contains 10–15% of the mixed $^{14}N,^{15}N$ species, a series of small peaks arising from this species show up in the spectrum. ^{15}N ENDOR spectra of **2** taken with three different field settings are depicted in Figure 4. With the center-field setting (E), four signals are observed, centered about an "average" $|a_{^{15}N}/2| = 70.5$ MHz. With the low-(D) and high-field (F) settings, however, only two of these signals are found. Furthermore, the signal intensities show a pronounced dependence on the field setting. In contrast to the situation described above for ^{14}N ENDOR of species **1**, the low-frequency signal is more intense with the low-field setting and vice versa for the high-field setting. Figure 5 demonstrates that the relative intensities of the ^1H ENDOR signals are also influenced when the field setting is switched (vide infra).

Second-Order Splittings. The most interesting feature in the ^{14}N ENDOR spectra of **1** (or in ^{15}N ENDOR of **2**) is certainly the finding that the ENDOR signals belonging to the two supposedly equivalent nitrogen nuclei show splittings. On the basis of a first-order treatment (eq 1), one might conclude that the two nitrogen nuclei are slightly inequivalent. However, a first-order treatment is not adequate in this case dealing with unusually large hyperfine coupling constants, and the consequences of second-order effects have to be taken into account. According to second-order perturbation theory, the energy level of state $|M_S,M_I>$ ($S = {}^1/_2$) is shifted by[11]

$$\delta E/h = (M_S a^2/2\nu_e)\{I(I+1) - M_I(M_I + 2M_S)\} \quad (2)$$

Maki et al. were the first to point out that second-order effects may give rise to splittings of ENDOR signals belonging to equivalent nuclei.[5] It was shown that it is appropriate to couple the individual nuclear angular momenta within the groups of equivalent nuclei thus forming subsets with total spin K, L, ..., etc.[12] The respective second-order correction is then given by

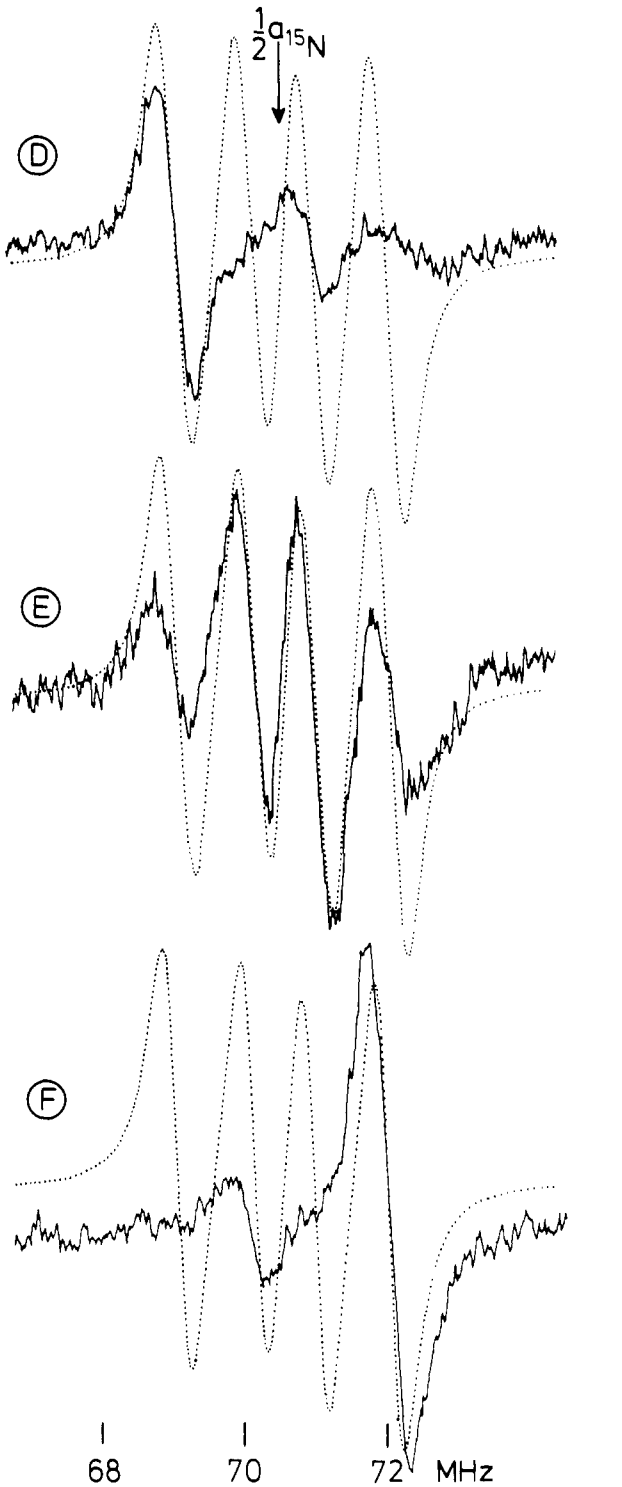

Figure 4. ^{15}N ENDOR spectra of **2** obtained with different field settings, cf. Figure 3: (D) low-, (E) center-, and (F) high-field setting (toluene/CF_3COOH, 230 K). The dotted spectra are computer simulations, see text.

eq 2, with I replaced by K, L, ... and M_I by the quantum numbers M_K, M_L, ... for the components of the nuclear group momenta along the direction of the field. The allowed nuclear transitions which give rise to ENDOR signals have the selection rules $\Delta M_S = 0$, $\Delta K = \Delta L = ... = 0$, and $\Delta M_K = \pm 1$ (or $\Delta M_L = \pm 1$, etc.). The ENDOR frequencies, correct to second order, are then given by[5]

$$\nu_{M_K \leftrightarrow M_K+1} = |-\nu_n + aM_S - (a^2 M_S/\nu_e)(M_K + M_S + {}^1/_2)| \quad (3)$$

where ν_n and ν_e are the free nuclear and electron Zeeman frequencies, respectively.

(11) Atherton, N. M. In "Multiple Electron Resonance Spectroscopy"; Dorio, M. M., Freed, J. H., Eds.; Plenum Press: New York, 1979; p149.
(12) Fessenden, R. W. *J. Chem. Phys.* **1962**, *37*, 747. Banerjee, M. K.; Das, T. P.; Saha, A. K. *Proc. R. Soc. London, Ser. A* **1954**, *A226*, 490.

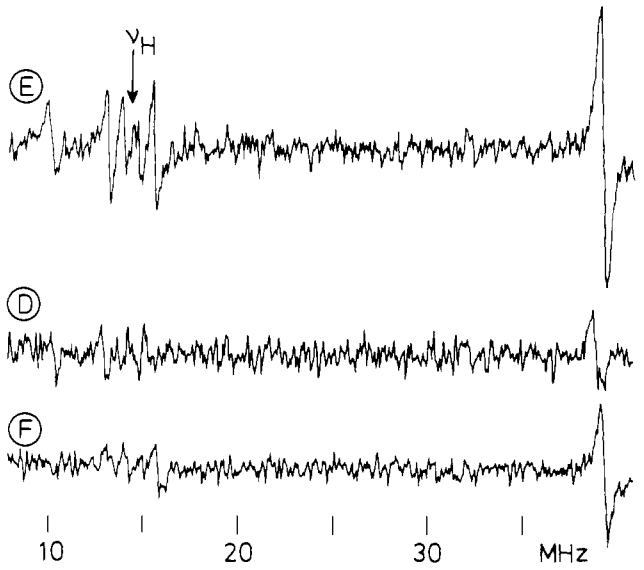

Figure 5. ^{1}H ENDOR spectra of **2** obtained with different field settings, cf. Figures 3 and 4 (toluene/CF_3COOH, 230 K).

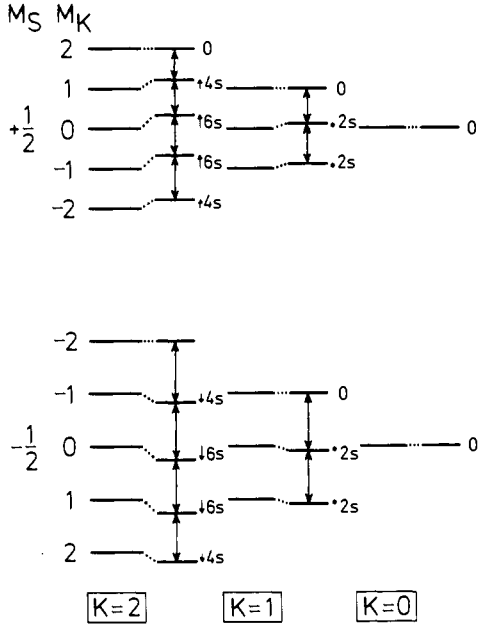

Figure 6. Energy level diagram of **1** showing second-order shifts of the hyperfine sublevels due to coupling with two equivalent ^{14}N nuclei. The nuclear spin states are grouped into subsets with total spin $K = 2$, 1, and 0, see text. The allowed NMR transitions are indicated.

To begin with the simpler case, the ^{15}N ENDOR experiment on **2** shall be considered first. Two equivalent ^{15}N nuclei ($I_{15_N} = {}^1/_2$) give rise to four nuclear spin states which can be grouped into a triplet ($K = 1$) and a singlet ($K = 0$) subset of equal weight. Since nuclear transitions are only allowed within each subset, only the triplet subset needs to be considered. Regarding the energy level scheme of the radical, each electron Zeeman sublevel ($M_S = -{}^1/_2, +{}^1/_2$) is split into a triplet by the nuclear Zeeman and hyperfine interactions. Whereas the two allowed nuclear transitions within each triplet are degenerate to first order, this degeneracy is lifted because of second-order effects (see Figure 6, middle column). The second-order shift s is defined by

$$s = a^2/4\nu_e \qquad (4)$$

Thus, a total of four distinct ^{15}N ENDOR signals is predicted for **2**. These are actually observed with the center-field setting (see Figure 4, center), i.e., when the desaturation of the EPR component belonging to $M_K = 0$ is monitored. With the low- or the high-field setting, either the EPR component belonging to $M_K = -1$ or that belonging to $M_K = 1$ is desaturated and only two of the ENDOR signals can be observed, arising from the transitions $|M_S,-1> \leftrightarrow |M_S,0>$ or $|M_S,0> \leftrightarrow |M_S,1>$. In order to give a quantitative account of the second-order shifts and splittings, the negative sign of the gyromagnetic ratio of ^{15}N has to be taken into consideration. Therefore ν_n in eq 1 and 3 must be replaced by $-|\nu_{15_N}|$, and sign $(a_{15_N}) = -$sign (a_{14_N}). Stick spectra demonstrating the influence of second-order shifts on the ^{15}N ENDOR line positions of **2** are given in Figure 7 (left). The observed second-order splitting of 1.10 MHz is in agreement with the calculated value, $2s = 1.05$ MHz. A computer simulation based on an exact diagonalization of the Hamiltonian matrix is depicted in Figure 4 (dotted spectra). It is assumed that all M_K components contribute equally, i.e., the simulation is given for the hypothetic experiment employing overmodulation of the EPR spectrum. In the actual experiments a selective desaturation takes place, therefore the simulation should be compared with a superposition of the three experimental spectra.

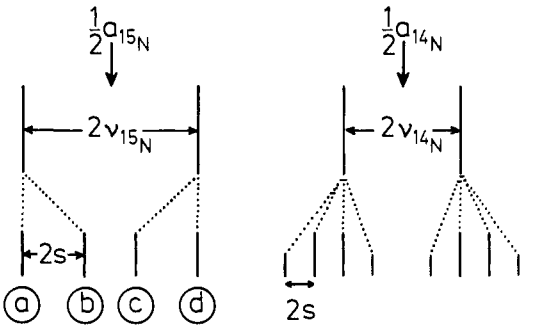

Figure 7. Stick spectra illustrating the second-order splittings in the ^{15}N ENDOR spectrum of **2** (left) and in the ^{14}N ENDOR spectrum of **1** (right). For comparison, the first-order spectra are also shown (top).

Table II. Calculated ^{14}N ENDOR Frequencies and Relative Intensities

transition intensity		frequency	
$M_K \leftrightarrow M_K + 1$		in $M_S = +{}^1/_2$	in $M_S = -{}^1/_2$
$1 \leftrightarrow 2$	1	$a_N/2 - \nu_N - 4s$	$a_N/2 + \nu_N - 2s$
$0 \leftrightarrow 1$	2	$a_N/2 - \nu_N - 2s$	$a_N/2 + \nu_N$
$-1 \leftrightarrow 0$	2	$a_N/2 - \nu_N$	$a_N/2 + \nu_N + 2s$
$-2 \leftrightarrow -1$	1	$a_N/2 - \nu_N + 2s$	$a_N/2 + \nu_N + 4s$

Regarding the ^{14}N ENDOR experiment on **1**, it should be noted that two equivalent ^{14}N nuclei ($I_{14N} = 1$) give rise to nine nuclear spin states which can be grouped into three subsets of equal weight with total spin $K = 2$ (quintet), $K = 1$ (triplet), and $K = 0$ (singlet). The degeneracy of states belonging to the same M_K but to a different subset is lifted by the second-order perturbation (see Figure 6). In this case, NMR transitions within the quintet subset and within the triplet subset have to be considered. The transition probabilities are given by eq 5,[13] where D denotes the degeneracy

$$P_{M_K \leftrightarrow M_K+1} \propto D\{K(K+1) - M_K(M_K+1)\} \qquad (5)$$

of the transition. The ENDOR frequencies and relative intensities for the system under consideration ($S = {}^1/_2$, $I_1 = I_2 = 1$) are summarized in Table II. Provided that all M_K components contribute equally to the ENDOR spectrum (in principle, achievable through overmodulation of the EPR spectrum during the ENDOR experiment), eight ENDOR signals should show up, exhibiting a second-order splitting of $2s = 0.53$ MHz, see Figure 7 (right) and the computer simulation given in Figure 2 (dotted spectra). This is just the experimentally observed splitting (0.56 MHz), but with the center-field setting, only four of these signals are found since mainly the $M_K = 0$ component is desaturated. However, the missing signals can be observed when the field setting is shifted to the low- or high-field portion of the EPR spectrum (see Figure 2). Unfortunately, the $M_K(^{14}N)$ components are

(13) Freed, J. H. In "Multiple Electron Resonance Spectroscopy"; Dorio, M. M., Freed, J. H., Eds.; Plenum Press: New York, 1979; p 73.

"mixed up" by the proton hyperfine interaction (six protons with $a_H \simeq a_N/2$), so that "pure" components are only available in the wings which are too weak for performing ENDOR experiments. Nevertheless, a quantitative analysis can be given when the individual contributions are taken into account, weighted by the degeneracy arising from the *proton* hyperfine interaction (e.g., center-field setting: $D(M_K = 0) = 20$, $D(M_K = \pm 1) = 6$). Hence the following intensity ratios are predicted for the eight possible ENDOR signals at the field settings A–C (cf. Figures 1 and 2): (A) 15:16:1:0:15:16:1:0, (B) 3:26:26:3:3:26:26:3, and (C) 0:1:16:15:0:1:16:15.

The second-order splittings of the ENDOR signals belonging to six equivalent protons with $a_H \simeq 50$ MHz can be explained analogously. The 64 proton spin states can be grouped into four subsets (the weight is given in parentheses): $K = 3$ ($D = 1$), $K = 2$ ($D = 5$), $K = 1$ ($D = 9$), and $K = 0$ ($D = 5$). It follows that two sextets of ^{1}H ENDOR signals are expected, with a second-order splitting of $2s = 0.13$ MHz and binomial intensity ratio (1:5:10:10:5:1) when all M_K components contribute equally. Actually only two doublets (splitting $\simeq 0.19$ MHz) are found experimentally with the center-field setting (see Figure 1, center). When the field is shifted, further ENDOR signals show up in much the same way as has been described above for ^{14}N ENDOR. However, in this case an appreciable change in the free proton Zeeman frequency (ν_H) has to be taken into account. Thus, when the field is shifted to position A or C (see Figure 1, top), the high-frequency doublet of ENDOR lines is shifted by 0.36 MHz toward lower or higher frequencies, respectively, and becomes unsymmetrical. Of this shift 0.24 MHz are due to the change in the free proton frequency. Second-order frequency shifts are also responsible for the fact that the spacing between the low- and high-frequency ^{1}H ENDOR signals is larger than $2\nu_H$, namely $2\nu_H + 2s$.

Cross-Relaxation Effects. It should be noted that second-order perturbation theory accounts for the splittings of ^{14}N and ^{15}N ENDOR signals but not for the asymmetric intensity pattern observed with off-center field settings (see Figures 2 and 4). Thus, high-frequency ^{14}N ENDOR signals are more intense than low-frequency signals when a low-field EPR component is desaturated and vice versa for a high-field setting, whereas the opposite behavior is found in the case of the ^{15}N ENDOR spectra. Considering the ^{14}N ENDOR experiment first, it can be stated that such behavior is usually found for ^{14}N atoms bearing a large π spin population. It has been reported, e.g., for nitroxides,[6,14] the pyrazine radical anion,[15] and a carbazolyl radical.[16] This phenomenon is due to cross-relaxation effects for simultaneous electron–nuclear spin flips, specifically, the contribution of W_{x2} (flop-flop) processes must be dominant.[6,17] The principle can be understood by means of the four-level scheme given in Figure 8, top left: When the low-field EPR component is desaturated, the high-frequency ENDOR signal should be enhanced if $W_{x2} > W_{x1}, W_n$. It is known from the theory of the ENDOR response that large cross-relaxation rates W_{x2} arise from the modulation of the electron–nuclear dipolar interaction ($W_{x2} = 6W_{x1}$).[13] Although it has been suggested that **1** should be described as a σ^* radical,[3] this does by no means imply that the bulk of the spin population resides in nitrogen 2s orbitals, but rather hybrid orbitals will be involved. Therefore, an appreciable electron–nuclear dipolar interaction of the nitrogen nuclei is expected in agreement with the experimental result.

The principal difference between ^{14}N and ^{15}N in this context is the fact that the gyromagnetic ratio of ^{14}N is positive, whereas that of ^{15}N is negative. Also the sign of the nitrogen hyperfine coupling is reversed when ^{14}N is replaced by ^{15}N. The appropriate four-level energy scheme for a radical exhibiting hyperfine interaction with a ^{15}N nucleus is given in Figure 8, top right. A

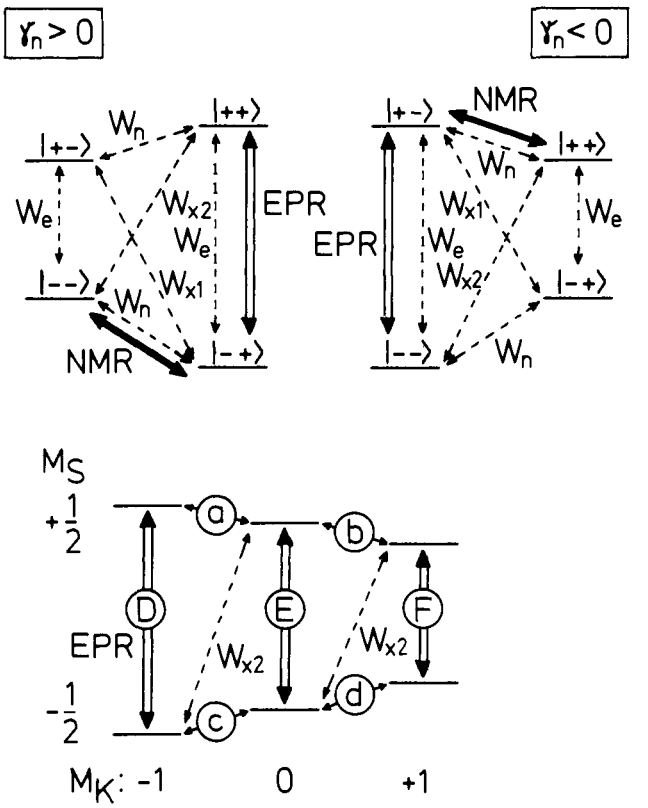

Figure 8. Top: Four-level energy schemes for doublet radicals ($S = {}^1/_2$) exhibiting hyperfine interaction with one nucleus ($I = {}^1/_2$) with $\nu_n > 0$, $a > 0$ (left) and $\nu_n < 0$, $a < 0$ (right); in both cases, $|a/2| > \nu_n$. The various relaxation paths are indicated. The low-field EPR transitions and the NMR transitions connected by W_{x2} processes are symbolized by arrows. Bottom: Energy level scheme for **2** showing the possible EPR and NMR transitions labeled in accordance with Figures 3 and 7 (left), respectively.

comparison with the diagram on the left-hand side demonstrates that the cross-relaxation processes W_{x1} and W_{x2} have changed their roles. Thus, the low-frequency ENDOR signal is enhanced when the low-field EPR component is desaturated provided that $W_{x2} > W_{x1}, W_n$. The diagram in Figure 8, bottom, serves to account for the ^{15}N ENDOR experiment under consideration (see Figure 4). From left to right, EPR transitions corresponding to the low-, center-, and high-field setting are indicated. The four possible NMR transitions are denoted by $a - d$ (cf. Figure 7, left), and the W_{x2} cross-relaxation paths are shown. Thus, with the low-field setting (D) ENDOR lines a and c can be observed with a being enhanced by W_{x2} processes, whereas with the high-field setting (F) ENDOR lines b and d should show up with d being enhanced. With the center-field setting (E) all four ENDOR lines can be observed, but now the signals b and c are enhanced.

Figure 5 demonstrates that the cross-relaxation effects due to the ^{15}N nuclei also influence the relative intensities of the ^{1}H ENDOR signals. It has been shown previously that this behavior is strictly analogous to a general TRIPLE experiment.[15,18] That means, ^{1}H ENDOR signal intensities will be enhanced if the respective NMR transitions occur in the same M_S manifold as that of the enhanced ^{15}N ENDOR signal. In the case of the ^{15}N nucleus, its negative gyromagnetic ratio has to be taken into account, therefore the rules for interpreting general TRIPLE spectra have to be reversed. Thus, when a nucleus with a positive gyromagnetic ratio (e.g., ^{14}N) is replaced by an isotope with a negative gyromagnetic ratio (e.g., ^{15}N), the sign of the hyperfine coupling constant is reversed (by definition) whereas low- and high-frequency NMR transitions still occur in the *same* M_S manifolds (cf. Figure 8, top). In the present case it is reasonable

(14) Kirste, B.; Krüger, A.; Kurreck, H. *J. Am. Chem. Soc.* **1982**, *104*, 3850.
(15) Lubitz, W.; Nyrönen, T. *J. Magn. Reson.* **1980**, *41*, 17.
(16) Kirste, B.; Kurreck, H. *Appl. Spectrosc.* **1980**, *34*, 305.
(17) Fey, H.-J.; Lubitz, W.; Zimmermann, H.; Plato, M.; Möbius, K.; Biehl, R. *Z. Naturforsch. A* **1978**, *A33*, 514.
(18) Hass, Ch.; Kirste, B.; Kurreck, H.; Schlömp, G. *J. Am. Chem. Soc.* **1983**, *105*, 7375.

to assume that the ^{14}N coupling constant of **1** is positive, hence the ^{15}N coupling in **2** is negative. An inspection of Figures 4 and 5 demonstrates that the ENDOR signal intensities of the largest proton coupling show the same behavior as the ^{15}N ENDOR signals. For the reasons discussed above, a positive sign must be assigned to this proton coupling constant which is in fact reasonable since these protons are in β positions to the nitrogen atoms implying a hyperconjugative mechanism of spin density transfer. Although the signal-to-noise ratio of the other ^1H ENDOR signals is rather poor, their intensity pattern is in agreement with the results deduced from a ^1H TRIPLE experiment (Table I).

Symmetry of the Radical Cation. From the discussion given above it is clear that the observed splittings of the ^1H, ^{14}N, and ^{15}N ENDOR signals are solely due to second-order effects and not to an asymmetry of the radical cation. The measured second-order splittings are even in quantitative agreement with the calculated values, i.e., a dynamic frequency shift[6] has not been discerned. Moreover, a modulation of the isotropic nitrogen hyperfine couplings should give rise to large W_{x1} (flip-flop) cross-relaxation rates,[13] whereas experimentally $W_{x2} > W_{x1}$ was found. At least on the time scale of the ENDOR experiment, the two nitrogen atoms are equivalent. A more sensitive test of the symmetry might be possible by asymmetric isotopic substitution, i.e., by investigation of the $^{14}N,^{15}N$ species. If the radical cation is truly symmetrical, this would give rise to isotopic perturbation of resonance,[19] and the parameters for the mixed system should be essentially the same as those of species **1** and **2**. On the other hand, if the radical cation is rapidly interconverting between two unsymmetrical structures, the isotopic perturbation of degeneracy might make the parameters for the mixed species appreciably different.[20] Although sample **2** should contain 10–15% of the $^{14}N,^{15}N$ species, the maximum intensity of resolved satellite lines in the EPR spectrum due to this species did not exceed 2% of the most intense EPR signal (see Figure 3). Therefore ENDOR spectra of the mixed species could not be obtained. Judging from the EPR spectrum, however, it can be said that the satellite lines occur exactly at the positions calculated from the data measured for **1** and **2**. Consequently any effects due to asymmetric isotopic labeling, if present at all, must be very small.

Conclusions

Concluding we can state that the appearance of second-order splittings has to be taken into account in ENDOR studies involving equivalent nuclei with large coupling constants. All evidence obtained so far supports the view that the N–N bond in the propellane-type radical cations under investigation is truly symmetrical. Furthermore, in this study a detailed account of the influence of the substitution of a nucleus with a positive gyromagnetic ratio (^{14}N) by an isotope with a negative gyromagnetic ratio (^{15}N) on the ENDOR spectra has been given. Thus, the sense of second-order shifts, the asymmetry of the intensity pattern caused by cross-relaxation effects, and the rules for interpreting general TRIPLE spectra are reversed.

Experimental Section

Instrumentation. EPR, ENDOR, and TRIPLE spectra were recorded on a Bruker ER 220D EPR spectrometer equipped with a Bruker cavity (ER200ENB) and home-built NMR facilities described elsewhere.[21] For ^1H ENDOR, an ENI A500 amplifier was used, whereas for ^{14}N and ^{15}N ENDOR (i.e., above 35 MHz) an ENI 350L amplifier was employed. Microwave power levels of 30–60 mW were applied and radio-frequency power levels of about 90 W (field strength of 0.4 mT in the rotating frame) for ^1H ENDOR and about 20 W (0.2 mT) for ^{14}N and ^{15}N ENDOR (not constant over the frequency range). ENDOR spectra were accumulated by using a Nicolet signal averager 1170 employing 1K data points; typically 128 sweeps were taken, 30 s per scan.

Synthesis of 1,6-Diazabicyclo[4.4.4]tetradecane-$^{15}N_2$ Radical Cation Tetrafluoroborate. The synthesis followed published procedures[4] for the most part, so that only differences of procedures and the results are given below.

3,6-Dihydroxypyridazine-$^{15}N_2$ (Maleic Hydrazide-$^{15}N_2$). The method closely follows a published procedure.[22] Hydrazine-$^{15}N_2$ sulfate ($^{15}N_2H_6SO_4$, 0.500 g, 95 atom % from Amersham International plc) and maleic acid (0.500 g) were dissolved in water (4 mL) and heated at 100 °C for 4 h. The reaction mixture was cooled to 0 °C and filtered. The crystals were washed with water, ethanol, and finally ether, and the product (0.369 g) was obtained as colorless plates. The filtrate was evaporated and the residue stirred with an ethanol (2 mL)/ether (4 mL) mixture, the insoluble white powder being more product (8 mg). The total yield was 88%.

1,6-Diazabicyclo[4.4.0]deca-3,8-diene-2,5-dione-$^{15}N_2$. The oxidation of maleic hydrazide-$^{15}N_2$ (0.377 g) with lead tetraacetate and trapping of the resultant diazaquinone was conducted as described by Clement.[23] After chromatography on alumina and elution with dichloromethane, 1,6-diazabicyclo[4.4.0]deca-3,8-diene-2,5-dione-$^{15}N_2$ was obtained as pale yellow crystals (0.477 g, 86%).

1,6-Diazabicyclo[4.4.0]decane-2,5-dione-$^{15}N_2$. The product from above (in 25 mL H_2O) was hydrogenated under a pressure of 3 bar for 2 h, with 0.3 g of Raney nickel catalyst, to give 1,6-diazabicyclo[4.4.0]decane-2,5-dione (0.419 g, 86%).

1,6-Diazabicyclo[4.4.0]decane-$^{15}N_2$. The hydrogenated product (0.225 g) was reduced with $LiAlH_4$ in tetrahydrofuran following the procedure of Stetter and Spangenberger[24] to give 0.173 g (93%) of crude bicyclic hydrazine which was used directly for the next stage.

1-(4-Bromobutyl)-1,6-diazabicyclo[4.4.0]decanium-$^{15}N_2$ Bromide and 1,6-Diazoniatricyclo[4.4.4.0]tetradecane-$^{15}N_2$ Bistetrafluoroborate. Alkylation of the bicyclic hydrazine (0.173 g) with 1,4-dibromobutane and cyclization with silver oxide in aqueous tetrafluoroboric acid was conducted as described previously,[4] yielding 0.313 g (71%) of bromo bromide intermediate and 0.241 g (74%) of the propellane dication salt.

1,6-Diazabicyclo[4.4.4]tetradecane-$^{15}N_2$ Radical Cation Tetrafluoroborate. 1,6-Diazoniatricyclo [4.4.4.0]tetradecane-$^{15}N_2$ bistetrafluoroborate (0.200 g) was reduced[4] with sodium in liquid ammonia to 1,6-diazabicyclo[4.4.4]tetradecane-$^{15}N_2$. Most of this material was converted into its inside protonated tetrafluoroborate salt (60% from the dication) for use in other experiments, but 10.2 mg was reacted with 1 equiv of 1,6-diazoniatricyclo[4.4.4.0]tetradecane-$^{15}N_2$ bistetrafluoroborate (19.3 mg) in dry CH_3CN (10 mL) during 6 h to furnish, after evaporation of the solvent, a quantitative yield of the radical cation salt.

Preparation of Samples. Samples were prepared by dissolving the trifluoromethanesulfonate of the radical cation **1** or the tetrafluoroborate salt of **2** in dichloromethane or a mixture of toluene and trifluoroacetic acid. The solutions were carefully deoxygenated prior to EPR/ENDOR measurements by flushing with purified N_2 or by means of the freeze–pump–thaw technique at a high-vacuum line.

Acknowledgment. We thank Dr. M. Plato (FU Berlin) for helpful discussions. H. K. gratefully acknowledges financial support by Deutsche Forschungsgemeinschaft (Normalverfahren) and Fonds der Chemischen Industrie. B.K. gratefully acknowledges a Liebig stipend of the Fonds der Chemischen Industrie. R.W.A. and R.B.S. thank the S.E.R.C. for support (Grant No. GR/CO2303).

Registry No. 1, 71058-67-8; **2**, 95617-12-2; N-15, 14390-96-6; N_2, 7727-37-9; hydrazine-$^{15}N_2$ sulfate, 88491-70-7; maleic acid, 110-16-7; 3,6-dihydroxypyridazine-$^{15}N_2$, 68315-34-4; 1,6-diazabicyclo[4.4.0]deca-3,8-diene-2,5-dione-$^{15}N_2$, 95617-13-3; 1,6-diazabicyclo[4.4.0]decane-2,5-dione-$^{15}N_2$, 95617-14-4; 1,6-diazabicyclo[4.4.0]decane-$^{15}N_2$, 95617-15-5; 1-(4-bromobutyl)-1,6-diazabicyclo[4.4.0]decanium-$^{15}N_2$ bromide, 95646-76-7; 1,6-diazoniatricyclo[4.4.4.0]tetradecane-$^{15}N_2$ bistetrafluoroborate, 95646-64-3; 1,6-diazabicyclo[4.4.4]tetradecane-$^{15}N_2$ radical cation tetrafluoroborate, 95617-17-7.

(19) Saunders, M.; Kates, M. R. *J. Am. Chem. Soc.* **1977**, *99*, 8071.
(20) Saunders, M.; Telkowski, L.; Kates, M. R. *J. Am. Chem. Soc.* **1977**, *99*, 8070.
(21) Kurreck, H.; Kirste, B.; Lubitz, W. *Angew. Chem.* **1984**, *96*, 171; *Angew. Chem., Int. Ed. Engl.* **1984**, *23*, 173.
(22) Feuer, H.; White, E. H.; Wyman, J. E. *J. Am. Chem. Soc.* **1958**, *80*, 3790.
(23) Clement, R. A. *J. Org. Chem.* **1962**, *27*, 1115.
(24) Stetter, H.; Spangenberger, H. *Chem. Ber.* **1958**, *91*, 1982.